coatings

MDPI

Article

Temperature-Independent Thermal Radiation Design Using Phase-Change Materials

Viktoriia E. Babicheva [1,*], Heungsoo Kim [2] and Alberto Piqué [2]

[1] Department of Electrical and Computer Engineering, University of New Mexico, MSC01 1100, 1 University of New Mexico, Albuquerque, NM 87131, USA
[2] Naval Research Laboratory, 4555 Overlook Ave, Washington, DC 20375, USA; heungsoo.kim.civ@us.navy.mil (H.K.); alberto.pique.civ@us.navy.mil (A.P.)
* Correspondence: vbb@unm.edu

Abstract: The ability to treat the surface of an object with coatings that counteract the change in radiance resulting from the object's blackbody emission can be very useful for applications requiring temperature-independent radiance behavior. Such a response is difficult to achieve with most materials except when using phase-change materials, which can undergo a drastic change in their optical response, nullifying the changes in blackbody radiation across a narrow range of temperatures. We report on the theoretical design, giving the possibility of extending the temperature range for temperature-independent radiance coatings by utilizing multiple layers, each comprising a different phase-change material. These designed multilayer coatings are based on thin films of samarium nickelate, vanadium dioxide, and doped vanadium oxide and cover temperatures ranging from room temperature to up to 140 °C. The coatings are numerically engineered in terms of layer thickness and doping, with each successive layer comprising a phase-change material with progressively higher transition temperatures than those below. Our calculations demonstrate that the optimized thin film multilayers exhibit a negligible change in the apparent temperature of the engineered surface. These engineered multilayer films can be used to mask an object's thermal radiation emission against thermal imaging systems.

Keywords: infrared; vanadium dioxide; samarium nickelate; insulator-to-metal transition; Planck thermal emission; thermal radiation; engineered emissivity coating

check for updates

Academic Editor: Lei Zhao

Received: 6 November 2024
Revised: 14 December 2024
Accepted: 25 December 2024
Published: 2 January 2025

Citation: Babicheva, V.E.; Kim, H.; Piqué, A. Temperature-Independent Thermal Radiation Design Using Phase-Change Materials. *Coatings* **2025**, *15*, 38. https://doi.org/10.3390/coatings15010038

Copyright: © 2025 by the authors. Licensee MDPI, Basel, Switzerland. This article is an open access article distributed under the terms and conditions of the Creative Commons Attribution (CC BY) license (https://creativecommons.org/licenses/by/4.0/).

1. Introduction

Thermal imaging systems, such as infrared thermal cameras, can detect the surface of remote objects by measuring their temperature profiles. Similarly, blocking thermal radiation against thermal imaging systems using active or passive temperature control systems is an ongoing research area to hide an object or individual from infrared detection [1–3]. Such systems are particularly advantageous against thermal imaging devices that detect heat signatures, and thermal technology encompasses a range of techniques and materials designed to make objects less detectable or even invisible to thermal detection methods. Hiding temperature information can be achieved by masking or mimicking the heat signature of the surrounding environment and is primarily used to avoid detection by thermal imaging cameras [2,3]. Efficient emission management can be achieved through insulation, cooling systems, or materials that emit radiation in a controlled manner. The challenge remains to develop a thermal system that works effectively in situations when the temperature difference is significant and in extremely hot or cold environments [4,5].

A conventional thermal emission from an object of a certain temperature, governed by the Stefan–Boltzmann law, limits versatility and controllability. Recent research has aimed to break this conventional relationship, offering a unique opportunity for thermal management and manipulation of energy transfer [6–10]. Phase-change materials commonly used in nanophotonics, such as vanadium dioxide VO_2 and germanium telluride, exhibit reversible transitions between different crystalline structures or amorphous/crystalline states, leading to significant changes in their optical properties [1–3,11–22]. However, hysteresis in phase-change materials poses a challenge due to the difficulty in precisely controlling the transition thresholds between the insulating and metallic states [23–26]. This hysteresis can result in inconsistent and unpredictable performance, complicating the design and optimization of devices relying on these materials. Doped VO_2 can make the transition less sharp, offering advantages such as smoother thermal responses, reduced hysteresis effect, and improved material stability.

The phase-change materials enable efficient dynamic tuning of the photonic properties of the nanostructure or device because of the light control at the nanoscale. Several recent works have reported on the development of phase-change materials and coatings based on these materials that mitigate conventional temperature-dependent properties of the surface [2,3,27,28]. The efforts have been directed towards creating a versatile coating capable of dynamically adjusting its emissivity in a broad temperature range, potentially enhancing its performance in thermal management, sensing, energy conversion technologies, thermophotovoltaics, and other applications [12,29,30].

Phase-change materials have been widely explored for controlling thermal emission, with the metal and dielectric phases of VO_2 exhibiting key properties that enable tunable thermal emissivity. Vanadium dioxide VO_2 transforms from a metallic phase at higher temperatures to an insulating phase as it cools below approximately 70 °C, and the properties of this material have been investigated extensively in recent years [31,32]. The phase-transition shift in electronic behavior is accompanied by abrupt changes in the conductivity and optical properties. VO_2 is highly suitable for smart radiation devices due to its sharp infrared reflectance change across its phase-transition temperature. Recent results have shown that a multilayer thin-film emitter, composed of a titanium nitride bottom infrared mirror, dielectric spacer, and a VO_2 top absorbing film, can efficiently control thermal emissivity through the phase transition of the VO_2 film [16]. Experiments reveal that a structure with a thin VO_2 film achieves a significant emissivity change ($\Delta\epsilon \cong 0.46$) across the temperature range corresponding to the material phase transition. Thus, VO_2 has the potential to be used in various applications ranging from smart coatings to energy-efficient devices [1,11–16].

Several phase-change materials beyond VO_2, such as germanium telluride and indium antimonide telluride alloys [33–35], have been explored extensively. These materials are widely used in various applications due to their ability to switch between amorphous and crystalline states, significantly altering their electrical and optical properties. Germanium telluride, for example, is commonly used in data storage technologies such as rewritable optical discs and nonvolatile memory devices. Indium antimonide telluride is another phase-change material known for its rapid switching speed and low power consumption, making it suitable for advanced data storage and memory applications [34]. However, a significant drawback of these materials for thermal applications is their requirement for substantial cooling to reverse the phase transition, which can be highly impractical and limits their efficiency in dynamic thermal management systems.

The phase transition of a material drastically alters its thermal and electrical properties and influences its ability to emit thermal radiation at various wavelengths. The emitter surface can be designed to counteract changes in the blackbody radiation distribution

over a specific temperature range, enabled by the insulator-to-metal phase transition. Samarium nickelate $SmNiO_3$ exhibits a metal-insulator transition around 120 °C and is considered a promising candidate for temperature-independent thermal radiation and infrared emission management [2,3,19]. $SmNiO_3$ is a strongly correlated quantum material that experiences a fully reversible, temperature-driven, solid-state phase transition. The smooth and hysteresis-free behavior of this insulator-to-metal phase transition allows engineering of the temperature dependence and cancels out intrinsic blackbody radiation spectra determined by the Stefan–Boltzmann law [3].

Here, we report on an advanced engineered coating that achieves thermal emission management of a surface using materials that undergo an insulator-to-metal phase transition and optical properties that can be drastically tuned with temperature. Our modeling demonstrates the potential for broadening the temperature range in which thermal emission management is achieved by employing multiple layers of phase-change materials. We use thin films of $SmNiO_3$ and VO_2 to compensate for the effect of the radiance change determined by the blackbody term. The surface's emissivity is drastically altered by the material's phase transition, which occurs at a different temperature for each layer. The effect of the coating thickness is investigated with the objective of achieving a minimal change in the apparent temperature of the engineered surface. Furthermore, we show that tungsten-doped VO_2 films reduce the temperature at which this negligible change occurs down to room temperature. The material with the lowest phase transition temperature is placed at the bottom, while the topmost layer has the highest phase transition temperature. Each successive layer has a higher phase transition temperature than the one below it, ensuring optimal performance. We demonstrate an effective thermal coating that spans from room temperature to above 140 °C using a multilayer comprising thin films of $SmNiO_3$ and doped VO_2.

2. Methods

The total amount of power emitted thermally by an object can be determined by integrating its spectral radiance—defined by Planck's law and emissivity—across all wavelengths and hemispherical angles. Assuming a negligible angular dependence of emissivity and integrating the angular dependency into the blackbody distribution, $I_{BB}(\lambda,T)$, this relationship can be written as

$$A \int_0^\infty d\lambda \varepsilon(\lambda, T) I_{BB}(\lambda, T) = A\varepsilon_{tot}(T)\sigma T^4, \quad (1)$$

where A represents the surface area, $\epsilon(\lambda,T)$ denotes the spectral emissivity, λ is the wavelength in free space, T is the temperature, and σ is the Stefan–Boltzmann constant. The total emissivity, $\epsilon_{tot}(T)$, may exhibit some degree of temperature dependence even in cases when the spectral emissivity does not, due to the integration of $\epsilon(\lambda)I_{BB}(\lambda,T)$. However, this effect is generally overshadowed by the T^4 term, allowing ϵ_{tot} to be approximated as a constant. Therefore, the Stefan–Boltzmann law establishes a direct connection between the temperature of a surface and its emitted radiation, affirming the common understanding that hotter surfaces emit more power. This principle can be used in devices for infrared imaging and contactless thermometry. It is possible to break this direct connection between temperature and emitted thermal power using an engineered-thermal-emission coating. The ideal coating acts as an emitter of a consistent amount of radiation regardless of its temperature, which can obscure the detection of temperature variations across a surface from infrared imaging devices. This kind of emitter has been called a zero-differential emitter, followed by further analysis of whether it conceals thermal signatures in a broad range of wavelengths or at specific spectral points [2,3]. In one case, the thermal emission

from one such coating is of approximately the same power at various temperatures if integrated over a particular wavelength range [2]. Concealment of thermal signatures from hyperspectral cameras and bandpass filters can be realized using zero-differential spectral emitters, where changes in blackbody radiation at each wavelength are offset by changes in emissivity at the same wavelength [3].

The figure of merit (FoM) of the thermal coating operating based on the zero-differential spectral emitter can be defined in the following way [3]:

$$\mathrm{FoM} = \int_{\lambda_1}^{\lambda_2} \frac{1}{I(\lambda,\ T)} \frac{\partial I(\lambda,\ T)}{\partial T}\ d\lambda, \tag{2}$$

where $I(\lambda,T)$ is the emitted temperature-dependent spectral radiance that corresponds to any object emitting thermal radiation, and $I(\lambda,T) = \epsilon(\lambda) I_{BB}(\lambda,T)$. This FoM reflects the degree of change in the emitted temperature-dependent radiance for an infinitesimal change in temperature, normalized to the initial radiance. As it is a spectrally-dependent characteristic, it is integrated over the spectral range of interest. This FoM needs to be minimized to obtain a coating with minimal changes in the radiance with respect to temperature variations.

The calculation of FoM takes into account not only the contribution of blackbody radiation $I_{BB}(\lambda,T)$ but also the impact of the emissivity of the coating $\epsilon(\lambda)$. Emissivity plays a crucial role in determining the efficiency with which a material can radiate energy as thermal radiation. Since the emissivity varies with both the material properties and the surface characteristics, it influences the overall energy emission and absorption behavior. Therefore, for a comprehensive assessment of FoM, both blackbody radiation principles and the specific emissivity values must be incorporated, ensuring that the material's radiation efficiency is accurately accounted for in the design or analysis. Calculations of the emissivity of a coating made of multiple layers are performed using the transfer-matrix method, and emissivity is determined from the reflectance of the multilayer structure. Our model accounts for the materials' dispersion and change with respect to temperature and doping. In our analysis, we consider an Al:ZnO (AZO) layer deposited on an infinitely thick SiO_2 substrate. AZO was selected as a reflective layer because its optical properties are similar to those of indium tin oxide (ITO). AZO does not contain expensive materials such as indium, which means that AZO is a more affordable option than ITO for large-area applications. In contrast to highly reflective silver, AZO withstands the high-temperature processes required for the deposition of the oxide phase-change materials selected for our engineered coatings.

3. Results

3.1. Engineered Multilayer Coatings

The changes corresponding to the typical unconcealed thermal signatures of the hot object are determined primarily by changes in blackbody radiation (Figure 1a). The spectral radiances of the substrate for different temperatures are shown in Figure 1b. The emissivity of the SiO_2 surface in the same wavelength range remains constant with temperature due to the negligible change in the refractive index of SiO_2. As expected from the Stefan–Boltzmann law, hotter surfaces emit more power and appear unconcealed, as the emission increases drastically with the temperature.

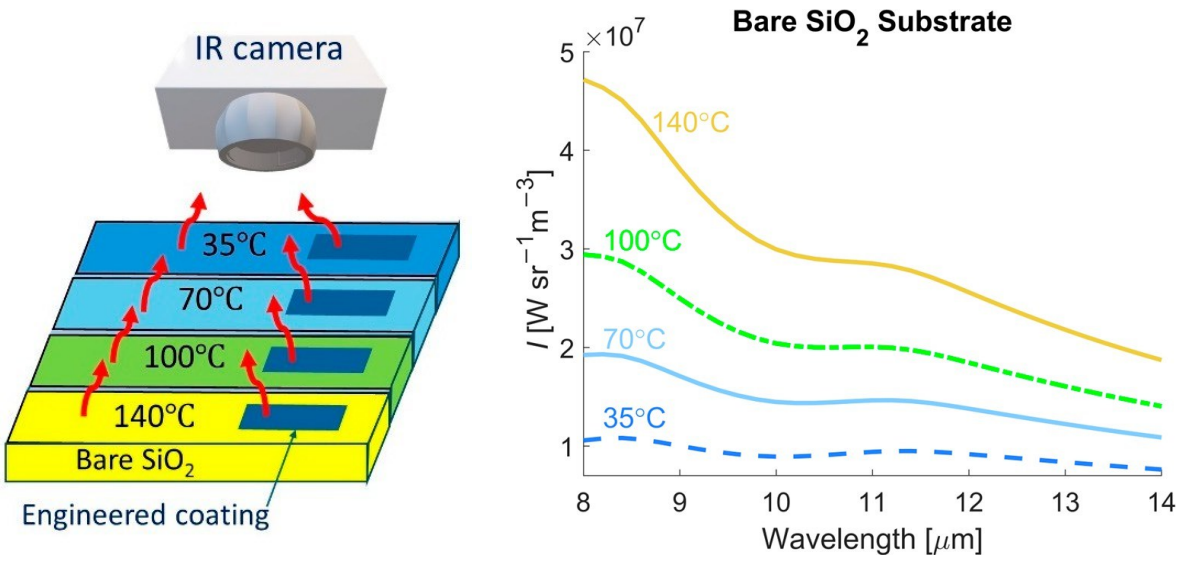

Figure 1. (**a**) Schematic illustrating the thermal concealment of a hot surface. The unconcealed surface appears to have different temperatures upon heating. In contrast, the ideal concealed surface appears to have the same temperature with low radiance, even when the actual temperature of the surface is increased. (**b**) Spectral radiances of a SiO_2 substrate for different temperatures (35, 70, 100, and 140 °C). The plot shows typical unconcealed thermal changes determined primarily by changes in blackbody radiation.

Using the FoM definition with Equation (2), we first analyze the performance of individual $SmNiO_3$ or VO_2 layers on AZO/SiO_2. We find that a 250 nm thick layer of AZO generally provides sufficient reflection as the bottom layer of the proposed zero-differential emitter. The thickness of the AZO remained fixed throughout this work since further increasing the thickness of the AZO layer does not improve the performance. In the reflectance calculations for determining the emissivity, wave absorption occurs almost entirely within approximately 250 nm of the AZO layer, and the thicker layer does not change the emissivity. The AZO permittivity is obtained by ellipsometry measurements (the case of 10 mTorr, reported in [36], along with the Drude fit in the extended spectral range). The spectral range of interest is 8–14 μm, and unless otherwise stated, the integration in the FoM definition is performed over this wavelength range.

The variation of the thickness of $SmNiO_3$ shows that FoM is minimum for the layer > 200 nm (Figure 2a). Data for the temperature-dependent refractive index of $SmNiO_3$ in the infrared range are taken from [2]. In the range of temperatures of 100–140 °C, $SmNiO_3$ undergoes a phase transition with a drastic change in material response and the ability to compensate for the change in blackbody radiation (arising from the multiplier I_{BB} in spectrally-dependent radiance and the FoM defined through it). The spectral emissivity is highest for low temperature and short wavelength and changes gradually (Figure 2b).

Similarly, a single layer of VO_2 results in substantial variations in FoM due to the compensation (dark blue) or overcompensation (dark red) of the blackbody radiation (Figure 2c). Temperature-dependent refractive-index data of VO_2 are taken from [14]. FoM is minimal for a layer thickness of around 450 nm, but there are rapid variations in the temperature range of 45–70 °C. The spectral emissivity changes rapidly in the range of temperatures corresponding to the phase transition (Figure 2d). These demonstrations of minimizing the thermal response by using the layers of phase-change materials open the possibility of designing a multilayer coating that covers a broader range of temperatures where effective emission management can be achieved, which we discuss below.

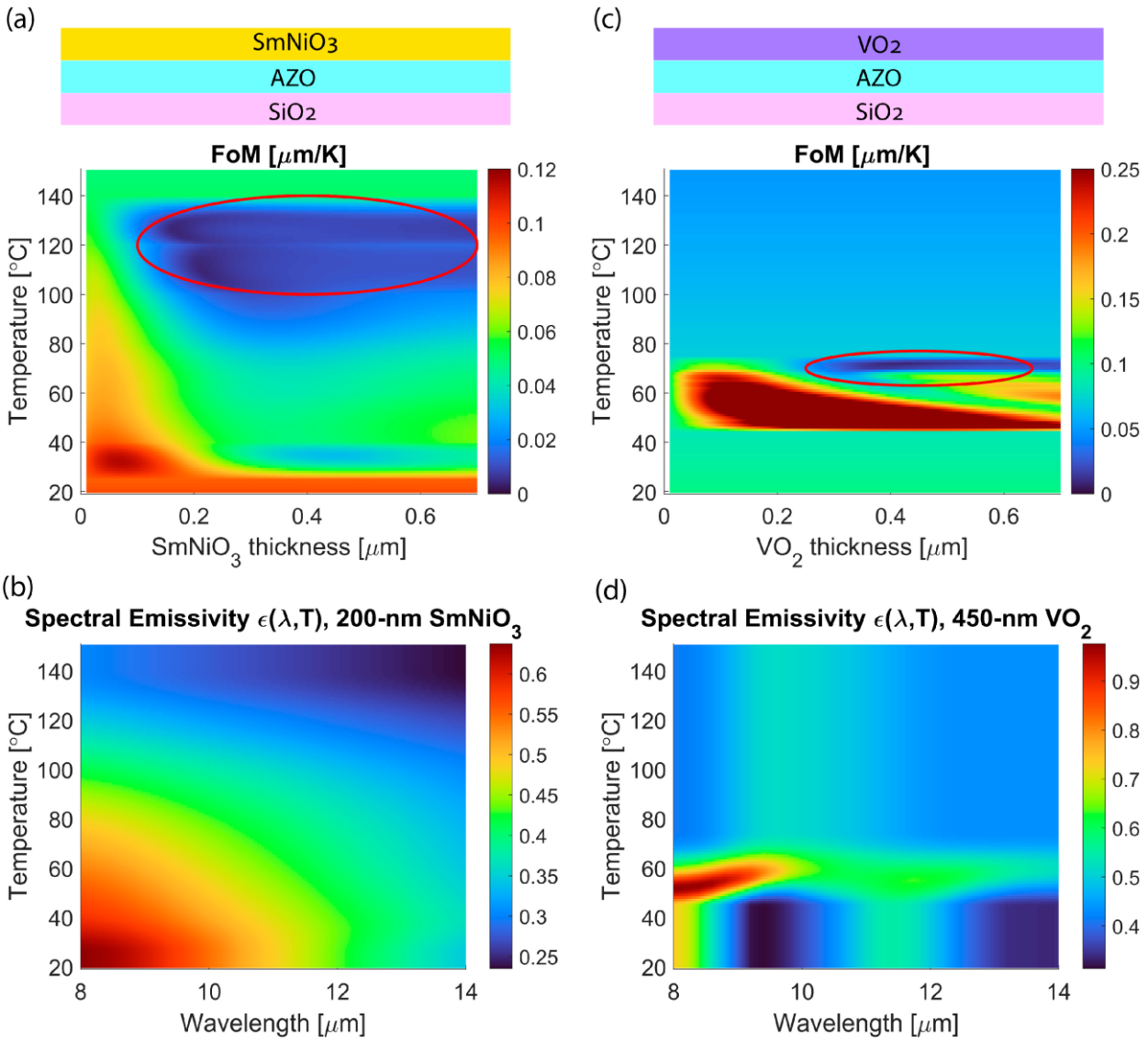

Figure 2. Effect of one layer of phase-change material on emitted radiance. (**a**,**b**) $SmNiO_3$ and (**c**,**d**) VO_2 on AZO/SiO_2. (**a**) $SmNiO_3$ minimizes FoM in the temperature range of 100–140 °C, which corresponds to its phase transition, and the ideal thickness of $SmNiO_3$ is >200 nm, denoted by a red circle. (**b**) Spectral emissivity of the coating with 200-nm $SmNiO_3$. (**c**) VO_2 strongly affects the radiance at temperatures around 45–70 °C, and the ideal thickness of VO_2 is approximately 450 nm, indicated by a red circle. (**d**) Spectral emissivity of the coating with 450-nm VO_2.

To extend the temperature range where the thermal coating operates, we engineer the multilayer coating using both $SmNiO_3$ and VO_2. A critical design principle is related to the order of the layers. The emissivity is determined from the reflectance of the multilayer structure, and the reflectance needs to take into consideration the phase transition temperature in each of the layers of the multilayer structure. Thus, in reflectance calculations, light should first reach the layer with the highest transition temperature and last propagate through the layer with the lowest transition temperature. The reason is that the material at temperatures above the transition temperature behaves as a metal and does not transmit light. Instead, the material is a dielectric below the transition temperature, allowing light to be transmitted through it with minimal losses.

Taking into account the design principle related to the order of each phase-change material, we engineer the multilayer coating where the $SmNiO_3$ and VO_2 layers are deposited on the AZO-coated SiO_2 substrate (Figure 3). Variations of each layer thickness

show that layers of around 200 nm are ideal. The combined effect of the $SmNiO_3$ and VO_2 layers extends the operating temperature range of the infrared coating from around 35 °C and up to 140 °C. Extending the performance of the multilayer coating across a broader temperature range enables better management of the emissivity over a wider temperature window.

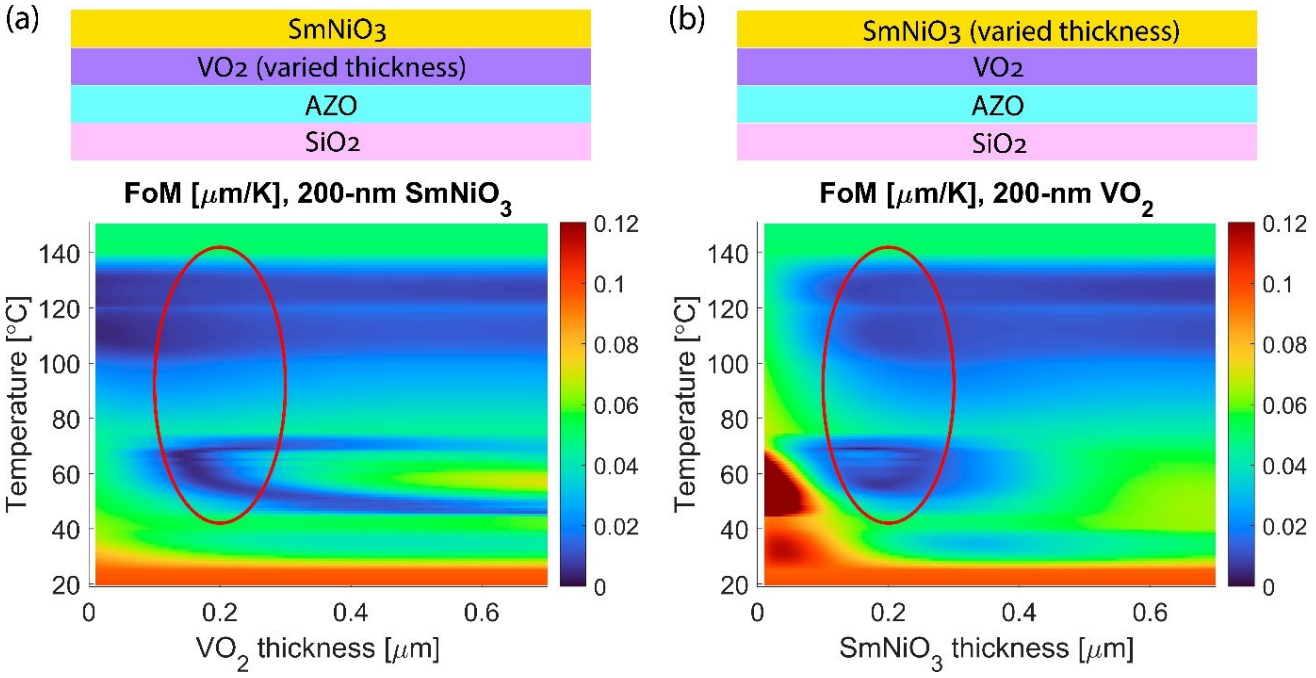

Figure 3. FoM for a combination of $SmNiO_3$ and VO_2 layers. The combination of layers extends the operating temperature range of the operation. Variations in the thickness of (**a**) VO_2 and (**b**) $SmNiO_3$. In both cases, the optimal thickness is approximately 200 nm (denoted red circles).

3.2. Further Multilayer Enhancements

Doping VO_2 with various elements can effectively control its metal-insulator transition temperature and properties [14,37–41]. Doping the VO_2 lattice with high-valence metal transition ions, such as W^{6+}, Mo^{6+}, or Nb^{5+}, strongly affects the transition temperature, reducing it for some doping and making the transition less sharp. Similarly, low-valence metal ions, such as Cr^{3+}, Al^{3+}, Fe^{3+}, or Ga^{3+}, have been shown to achieve a higher temperature of phase transition. Some other approaches, including doping of VO_2 with titanium, can stabilize the transition characteristics. These dopants alter the electronic structure and lattice parameters of VO_2, influencing its phase transition behavior and expanding its potential applications in thermochromic smart windows and other technologies. Although the transition temperature change is demonstrated with doping, complex refractive index data dependent on the temperature in the long-wave infrared range are rarely reported. We use data from [14] for W-doped VO_2 with W/V = 0.93 at. %, which has been shown to reduce the transition temperature by around 20 degrees, reaching temperatures below 40 °C. The three-layer phase-transition material coating can further reduce the temperature of thermal emission management (Figure 4a). Figure 4b shows a comparison of the best coatings in each category, clearly indicating that additional layers can result in the extension of the temperature range. For these calculations, the film thicknesses are the following: $SmNiO_3$-only is shown for >200 nm; VO_2 and $SmNiO_3$ combination is shown for each layer of 200 nm; and finally, a bilayer of VO_2 with $SmNiO_3$ is for 150-nm VO_2, 200-nm W:VO_2, and 200-nm $SmNiO_3$.

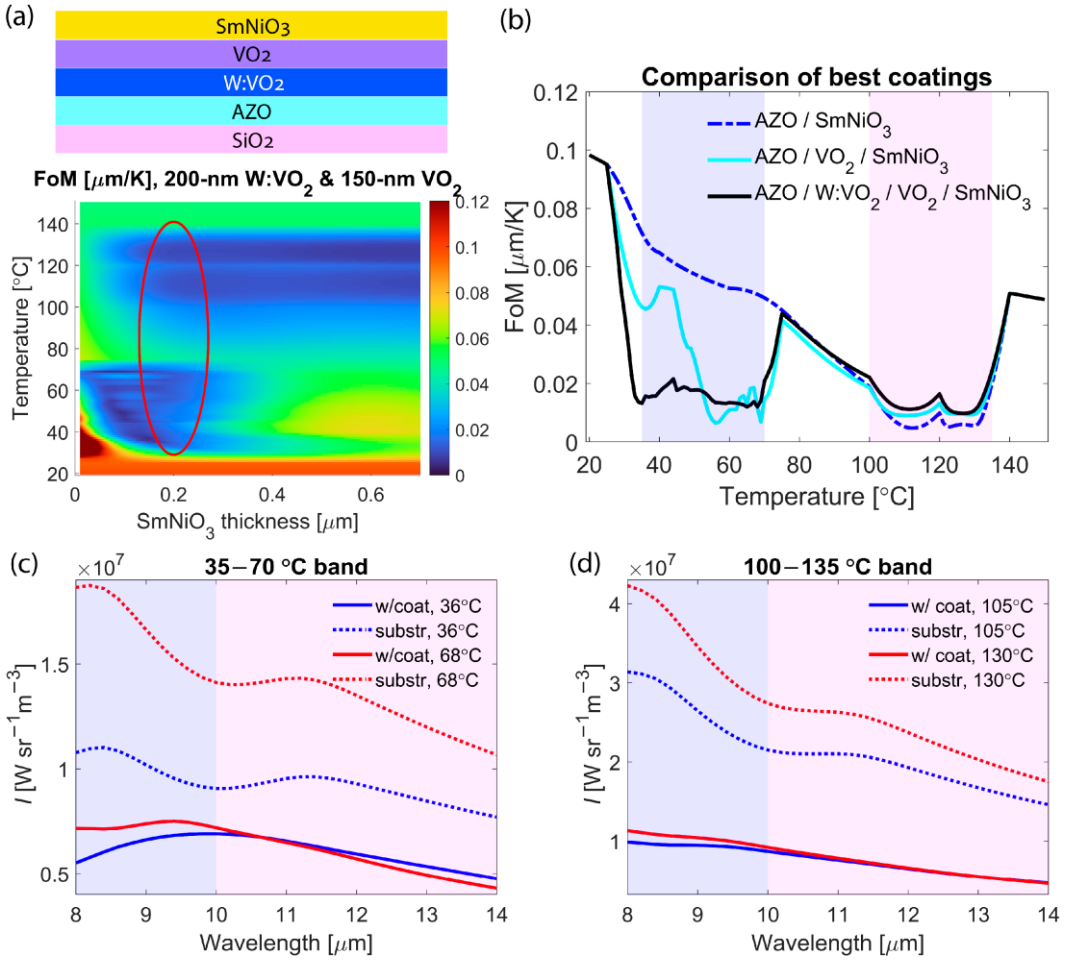

Figure 4. Further extension of the temperature range achieved with W doping of VO_2. (**a**) FoM for three layers of materials, $SmNiO_3$, VO_2, and W:VO_2 (0.93 at. %), changing the phase at different temperatures. The red circle shows the optimal range of $SmNiO_3$ thickness. (**b**) Comparison of FoMs for the best coating in each category. $SmNiO_3$ works only in one band (100–135 °C). Adding layers of VO_2 extends the effect to lower temperatures (35–70 °C). (**c**,**d**) Spectral radiances for the lower and higher temperature bands, respectively. The comparison is shown for engineered coating ($SmNiO_3$, VO_2, and 0.93 at. % W:VO_2, solid lines) and bare SiO_2 substrate (dotted lines). The wavelength range is approximately divided into two ranges, and the range of 10–14 μm shows a much better performance of thermal emission management than 8–10 μm.

To illustrate the operation of a near-zero differential temperature coating, we demonstrate a negligible change in the spectral radiance *I* with temperature variation (Figure 4c,d). We observe that in each temperature band, 35–70 °C and 100–135 °C, variations are very small, except for the wavelength range of 8–10 μm (solid line in Figure 4c,d). For comparison, we show that the radiance of the SiO_2 substrate changes more drastically (dotted lines in Figure 4c,d). We approximately divide the entire wavelength range into 8–10 μm and 10–14 μm, and we calculate FoM for multilayer structures in each range (Figure 5a,b). One can observe that qualitatively, the tendency is the same, but the thermal coating performs better in the range of 10–14 μm. Comparing the spectral emissivity of two optimal coatings, which are VO_2 and $SmNiO_3$ combination and the bilayer of VO_2 with $SmNiO_3$ (Figure 5c,d), one can see a more gradual change for the latter, providing a better performance of the engineered coatings.

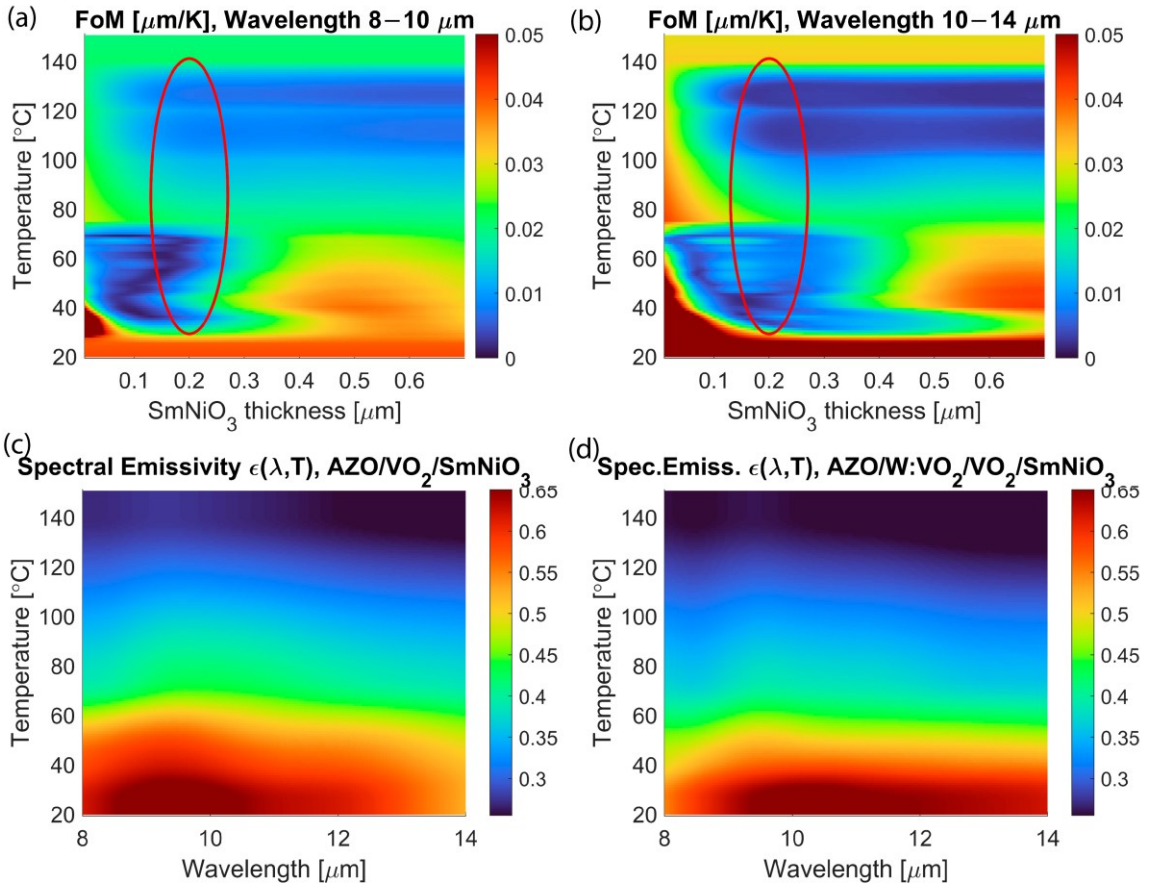

Figure 5. (**a**,**b**) Performance of the engineered emitter ($SmNiO_3$, VO_2, and 0.93 at. % W:VO_2) in different wavelength ranges of operation: (**a**) range 8–10 μm and (**b**) range 10–14 μm. Thermal coating is better if detection is performed only in the long-wave infrared range. The red circles in (**a**,**b**) show the optimal range of $SmNiO_3$ thickness. (**c**,**d**) Spectral emissivity of multilayer coatings: (**c**) VO_2 and $SmNiO_3$ combination is shown for each layer of 200 nm, and (**d**) bilayer of VO_2 with $SmNiO_3$ is for 150-nm VO_2, 200-nm W:VO_2, and 200-nm $SmNiO_3$.

Figures 4 and 5 illustrate that within the temperature range of 70–100 °C, a FoM peak is observed for all combinations of coating films. Potential solutions to optimize performance within this temperature range could involve exploring alternative materials with tailored properties, and the operation temperature of the thermal coating can be extended by utilizing materials with phase transition at other temperatures. It has been reported that doping with low-valence metal ions increases the transition temperature of VO_2, and these materials can be used to cover an additional temperature range of operation [42]. The transition temperature of VO_2 can be adjusted by incorporating low-valence metal ions, offering the potential to achieve temperatures suitable for broader operational ranges. This adaptability allows VO_2-based materials to extend their functionality across additional spectral bands. Rare-earth nickelates have been reported to exhibit transition temperatures that vary with material combination, the number of layers and their thickness, and other parameters [42–47]. Developing artificially phase-separated systems, such as epitaxial superlattices combining $SmNiO_3$ and $NdNiO_3$, provides a versatile platform for engineering transition temperatures. These are promising candidates for use in engineered coatings and structures for applications in infrared emission management and thermal applications. The ability to fine-tune these temperatures arises from the dependence of the phase transition on the specific composition of rare-earth nickelates, paving the way for coatings with expanded and customizable operational capabilities.

Finally, we present a comparative analysis of the spectral radiance for both unconcealed and concealed surfaces (Figure 6). Our calculations include an SiO_2 substrate and an optimized engineered emitter composed of three material layers $SmNiO_3$, VO_2, and $W:VO_2$ (0.93 at. %) layered on an AZO/SiO_2 substrate. The multilayer engineered surface demonstrates significantly enhanced performance, making it an excellent candidate for thermal applications. Analyzing spectral radiance is crucial to understanding how different materials emit thermal radiation and is essential for developing effective thermal technologies. The engineered surface substantially reduces spectral radiance, decreasing it several times compared to the unconcealed surface, thereby significantly improving its ability to evade detection by thermal imaging systems. This work demonstrates the potential for significant improvement in coating performance using a multilayer structure, with analyzed variations in parameters, while emphasizing the proof of optimality through extensive optimization is beyond its scope.

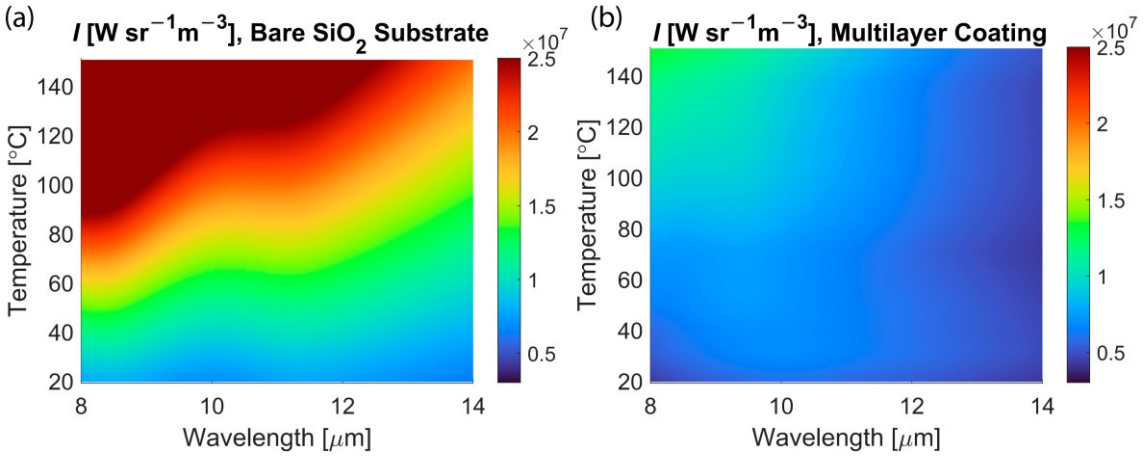

Figure 6. Comparison of the spectral radiance of unconcealed and concealed surfaces. (**a**) Calculations for the SiO_2 substrate and (**b**) for the optimized engineered emitter consisting of three layers of materials, $SmNiO_3$, VO_2, and $W:VO_2$ (0.93 at. %), on top of the AZO/SiO_2 substrate. Both maps are presented with the same color bar to show the relative performance of the thermal coating.

4. Discussion

Phase-change materials are promising candidates for engineered coatings and structures for infrared emission management and thermal applications. The temperature range where zero-differential emission from the object and coating occurs can be adjusted by modifying the material's strain, doping, or tilt, thereby shifting the transition to encompass room temperature and even lower temperatures (Figure 7). The dopants in VO_2 modify its electronic structure and lattice parameters, affecting its phase transition characteristics. Doping VO_2 with different elements allows the metal-insulator transition temperature and properties to be effectively controlled.

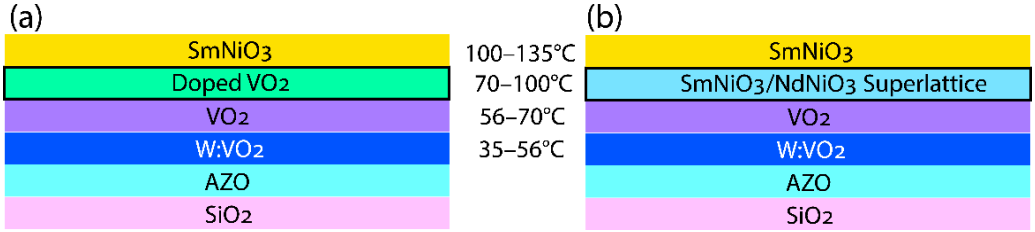

Figure 7. Multilayer engineered coatings that potentially cover the full range of temperatures, that is, from 35 °C to 135 °C: (**a**) design involving VO_2 doped with low-valence metal ions and (**b**) design involving epitaxial superlattices of $SmNiO_3$ and $NdNiO_3$.

Incorporating high-valence metal transition ions into the VO_2 lattice can lower the transition temperature. Thus, the operational temperature range can be extended by using multilayer stacks of materials with phase transitions at different temperatures. Low-valence metal ions can raise the transition temperature of VO_2, allowing these materials to cover an additional operational band (Figure 7a). Furthermore, doping VO_2 can soften the transition, providing more gradual thermal responses and improved material stability. This reduced sharpness can lead to better control over thermal management, which is highly beneficial for applications requiring the concealment of changes in temperature. This variability facilitates the design of zero-differential thermal emitters across a broad temperature range. The single-layer configuration that includes only $SmNiO_3$ can efficiently operate in the band of temperatures ~100–135 °C. The engineered multilayer structure proposed in this work is shown to expand the range of operation and include temperatures ~35–70 °C and ~100–135 °C. Using one or several layers of VO_2, including ones with doping, enhances the concealment coating and expands the operation temperature. This provides tailored phase-transition temperatures, steepness of the transition, and optical properties. Another benefit of using doped VO_2 systems is the associated reduction in their hysteresis.

Furthermore, the operation range of the engineered coating can potentially be extended using other materials and superlattices in the family of rare-earth nickelates (Figure 7b). Rare-earth nickelates have shown transition temperatures that vary based on material combinations, the number of epitaxial layers, and other factors [42,43]. In particular, an artificially phase-separated system can be atomically engineered by creating epitaxial superlattices with $SmNiO_3$ and $NdNiO_3$, two rare-earth compounds that experience metal-to-insulator transitions at different temperatures. The length scale of the interfacial interaction between the metal and insulator phases is controlled by balancing the energy expense of the boundary between these phases and the bulk phase energies. This length scale surpasses the physical coupling of structural motifs, introducing a new engineering approach for interface properties based on temperature rather than bulk energetics. Phase transitions at different temperatures have been studied extensively, but data on material permittivity in the mid-infrared range as a function of temperature remain unexplored. Calculations of advanced coatings involving engineered materials are beyond the scope of this work and will be the subject of future experimental investigations.

The thickness of each layer in a multilayer system is critical to the coating's overall performance. Optimizing the thickness of all layers simultaneously to achieve the best coating parameters is essential, and machine learning algorithms are well suited for this purpose. However, this optimization task lies beyond the scope of this work, and instead, we present an approach highlighting a concept that can be further refined through engineering the material properties of the multilayer structure.

5. Conclusions

This work shows how using a combination of thin film materials that exhibit pronounced insulator-to-metal phase transitions is possible to engineer coatings with temperature-independent radiance in an extended temperature range. These optical properties of the multilayer coating were designed to counter changes in the blackbody radiation from a SiO_2 substrate, showing the potential use of these coatings for applications calling for temperature-independent thermal radiation, infrared emission management, and cooling applications. Incorporating multiple layers of "zero-differential emitters (ZDE)" extends the operating temperature range. Our theoretical approach employed $SmNiO_3$, which undergoes a metal-insulator transition around 120 °C. Using a reversible and hysteresis-free $SmNiO_3$ phase transition helps to manage emissivity and mitigate intrinsic radiation profiles. The multilayer system included additional layers of VO_2, both undoped and

W-doped, which lowers the transition temperature. The results of our calculations showed that the temperature range of thermal emission management can be extended with these multilayer coatings, which consist of materials with transition temperatures covering a broad range. The coating is designed by adjusting both the thickness of each layer and the doping levels. In this multilayer engineered coating, the material that has the lowest temperature at which it undergoes a phase transition is strategically placed as the bottom layer. Furthermore, the material with the highest phase transition temperature is positioned at the topmost layer, ensuring optimal performance and efficiency. This design principle is consistently applied across all layers, meaning that each successive layer is made of a material with a progressively higher phase transition temperature than the one below it. A single-layer coating consisting of one phase-change material, $SmNiO_3$, is capable of functioning effectively within a temperature range of approximately 100–135 °C. We showed that incorporating an undoped VO_2 layer adds the band of 56–70 °C to the temperature operation. The best coating that we designed consists of 200 nm of $SmNiO_3$, 150 nm of undoped VO_2, and 200 nm of W:VO_2 (doping with W/V = 0.93 at. %) on top of a 250 nm thick layer of AZO on SiO_2 slab. Overall, the optimal multilayer structure with doped VO_2 expands the operational range to cover temperatures 35–70 °C and 100–135 °C.

Author Contributions: Conceptualization, V.E.B., H.K. and A.P.; Methodology, V.E.B., H.K. and A.P.; Validation, V.E.B. and H.K.; Formal analysis, V.E.B. and H.K.; Investigation, V.E.B., H.K. and A.P.; Resources, V.E.B. and H.K.; Data curation, V.E.B.; Writing—original draft, V.E.B., H.K. and A.P.; Writing—review & editing, V.E.B., H.K. and A.P.; Supervision, H.K. and A.P.; Project administration, H.K. and A.P.; Funding acquisition, H.K. All authors have read and agreed to the published version of the manuscript.

Funding: This work was funded by the Office of Naval Research (ONR) through the Naval Research Laboratory Basic Research Program (Grant No. N0001424WX00013). V.E.B. acknowledges support through the ONR Summer Faculty Research Program and the National Science Foundation under Grant No. 2418519.

Institutional Review Board Statement: Not applicable.

Informed Consent Statement: Not applicable.

Data Availability Statement: The data that support the findings of this study are available from the corresponding author upon reasonable request.

Conflicts of Interest: The authors declare that they have no known competing financial interests or personal relationships that could have appeared to influence the work reported in this paper.

References

1. Liu, D.; Ji, H.; Peng, R.; Cheng, H.; Zhang, C. Infrared chameleon-like behavior from VO2(M) thin films prepared by transformation of metastable VO2(B) for adaptive camouflage in both thermal atmospheric windows. *Sol. Energy Mater. Sol. Cells* **2018**, *185*, 210–217. [CrossRef]
2. Shahsafi, A.; Roney, P.; Zhou, Y.; Zhang, Z.; Xiao, Y.; Wan, C.; Wambold, R.; Salman, J.; Yu, Z.; Li, J.; et al. Temperature-independent thermal radiation. *Proc. Natl. Acad. Sci. USA* **2019**, *116*, 26402–26406. [CrossRef]
3. King, J.L.; Shahsafi, A.; Zhang, Z.; Wan, C.; Xiao, Y.; Huang, C.; Sun, Y.; Roney, P.J.; Ramanathan, S.; Kats, M.A. Wavelength-by-Wavelength Temperature-Independent Thermal Radiation Utilizing an Insulator–Metal Transition. *ACS Photonics* **2022**, *9*, 2742–2747. [CrossRef]
4. Kim, H.J.; Choi, Y.H.; Lee, D.; Lee, I.H.; Choi, B.K.; Phark, S.-H.; Chang, Y.J. Enhanced passive thermal stealth properties of VO2 thin films via gradient W doping. *Appl. Surf. Sci.* **2021**, *561*, 150056. [CrossRef]
5. Liu, D.; Cheng, H.; Xing, X.; Zhang, C.; Zheng, W. Thermochromic properties of W-doped VO2 thin films deposited by aqueous sol-gel method for adaptive infrared stealth application. *Infrared Phys. Technol.* **2016**, *77*, 339–343. [CrossRef]
6. Li, W.; Fan, S. Nanophotonic control of thermal radiation for energy applications [Invited]. *Opt. Express* **2018**, *26*, 15995–16021. [CrossRef] [PubMed]

7. Wang, J.; Tan, G.; Yang, R.; Zhao, D. Materials, structures, and devices for dynamic radiative cooling. *Cell Rep. Phys. Sci.* **2022**, *3*, 1011983. [CrossRef]
8. Baranov, D.G.; Xiao, Y.; Nechepurenko, I.A.; Krasnok, A.; Alù, A.; Kats, M.A. Nanophotonic engineering of far-field thermal emitters. *Nat. Mater.* **2019**, *18*, 920–930. [CrossRef]
9. Islam, M.S.; Babicheva, V.E. Lattice Mie resonances and emissivity enhancement in mid-infrared iron pyrite metasurfaces. *Opt. Express* **2023**, *31*, 40380–40392. [CrossRef]
10. Giteau, M.; Sarkar, M.; Ayala, M.P.; Enders, M.T.; Papadakis, G.T. Design Rules for Active Control of Narrowband Thermal Emission Using Phase-Change Materials. *Phys. Rev. Appl.* **2023**, *19*, L051002. [CrossRef]
11. Cueff, S.; John, J.; Zhang, Z.; Parra, J.; Sun, J.; Orobtchouk, R.; Ramanathan, S.; Sanchis, P. VO2 nanophotonics. *APL Photonics* **2020**, *5*, 110901. [CrossRef]
12. Kim, H.; Cheung, K.; Auyeung, R.C.Y.; Wilson, D.E.; Charipar, K.M.; Piqué, A.; Charipar, N.A. VO2-based switchable radiator for spacecraft thermal control. *Sci. Rep.* **2019**, *9*, 11329. [CrossRef] [PubMed]
13. Kim, H.; Bingham, N.S.; Charipar, N.A.; Piqué, A. Strain effect in epitaxial VO_2 thin films grown on sapphire substrates using SnO_2 buffer layers. *AIP Adv.* **2017**, *7*, 105116. [CrossRef]
14. Sun, K.; Wheeler, C.; Hillier, J.A.; Ye, S.; Zeimpekis, I.; Urbani, A.; Kalfagiannis, N.; Muskens, O.L.; de Groot, C.H. Room Tem-perature Phase Transition of W-Doped VO2 by Atomic Layer Deposition on 200 mm Si Wafers and Flexible Substrates. *Adv. Opt. Mater.* **2022**, *10*, 2201326. [CrossRef]
15. King, J.; Wan, C.; Park, T.J.; Deshpande, S.; Zhang, Z.; Ramanathan, S.; Kats, M.A. Electrically tunable VO2–metal metasurface for mid-infrared switching, limiting and nonlinear isolation. *Nat. Photonics* **2024**, *18*, 74–80. [CrossRef]
16. Kim, H.; Lahneman, D.; Rohde, C.; Piqué, A. VO2-based thin-film radiators with variable thermal emissivity. *Thin Solid Films* **2022**, *759*, 139455. [CrossRef]
17. Babicheva, V.E.; Lavrinenko, A.V. A plasmonic modulator based on metal-insulator-metal waveguide with barium titanate core. *Photonics Lett. Pol.* **2013**, *5*, 57–59. [CrossRef]
18. Babicheva, V.E.; Zhukovsky, S.V.; Lavrinenko, A.V. Bismuth ferrite as low-loss switchable material for plasmonic waveguide modulator. *Opt. Express* **2014**, *22*, 28890–28897. [CrossRef]
19. Khalichi, B.; Omam, Z.R.; Osgouei, A.K.; Ghobadi, A.; Ozbay, E. Polarization Insensitive Phase Change Material-Based Nano-antenna Array for Thermally Tunable Infrared Applications. In Proceedings of the 2022 IEEE International Symposium on An-tennas and Propagation and USNC-URSI Radio Science Meeting, Denver, CO, USA, 10–15 July 2022; pp. 687–688.
20. Wan, C.; Zhang, Z.; Woolf, D.; Hessel, C.M.; Rensberg, J.; Hensley, J.M.; Xiao, Y.; Shahsafi, A.; Salman, J.; Richter, S.; et al. On the Optical Properties of Thin-Film Vanadium Dioxide from the Visible to the Far Infrared. *Ann. Phys.* **2019**, *531*, 1900188. [CrossRef]
21. Huang, Y.; Zhang, D.; Liu, Y.; Jin, J.; Yang, Y.; Chen, T.; Guan, H.; Fan, P.; Lv, W. Phase transition analysis of thermochromic VO_2 thin films by temperature dependent Raman scattering and ellipsometry. *Appl. Surf. Sci.* **2018**, *456*, 545–551. [CrossRef]
22. Nagashima, M.; Wada, H. Near infrared optical properties of laser ablated VO_2 thin films by ellipsometry. *Thin Solid Films* **1998**, *312*, 61–65. [CrossRef]
23. Voloshenko, I.; Kuhl, F.; Gompf, B.; Polity, A.; Schnoering, G.; Berrier, A.; Dressel, M. Microscopic nature of the asymmetric hysteresis in the insulator-metal transition of VO_2 revealed by spectroscopic ellipsometry. *Appl. Phys. Lett.* **2018**, *113*, 201906. [CrossRef]
24. Jayswal, N.K.; Subedi, I.; Shan, A.; Podraza, N.J. Tracking optical properties of VOx films to optimize polycrystalline VO2 fab-rication. *Thin Solid Film.* **2024**, *798*, 140367. [CrossRef]
25. Kana, J.K.; Ndjaka, J.; Vignaud, G.; Gibaud, A.; Maaza, M. Thermally tunable optical constants of vanadium dioxide thin films measured by spectroscopic ellipsometry. *Opt. Commun.* **2011**, *284*, 807–812. [CrossRef]
26. Ramirez-Rincon, J.A.; Gomez-Heredia, C.L.; Corvisier, A.; Ordonez-Miranda, J.; Girardeau, T.; Paumier, F.; Champeaux, C.; Dumas-Bouchiat, F.; Ezzahri, Y.; Joulain, K.; et al. Thermal hysteresis measurement of the VO2 dielectric function for its metal-insulator transition by visible-IR ellipsometry. *J. Appl. Phys.* **2018**, *124*, 195102. [CrossRef]
27. Bos¸durmaz, E.B.; Ghobadi, A.; Özbay, E. Adaptive thermally tunable radiative cooling with angle insensitivity using phase-change-material-based metasurface. *Phys. Scr.* **2023**, *98*, 125948. [CrossRef]
28. Khalichi, B.; Ghobadi, A.; Osgouei, A.K.; Omam, Z.R.; Kocer, H.; Ozbay, E. Phase-change Fano resonator for active modulation of thermal emission. *Nanoscale* **2023**, *15*, 10783–10793. [CrossRef]
29. Hossain, M.M.; Jia, B.; Gu, M. A Metamaterial Emitter for Highly Efficient Radiative Cooling. *Adv. Optical Mater.* **2015**, *3*, 1047–1051. [CrossRef]
30. Li, Z.; Zhou, Y.; Qi, H.; Pan, Q.; Zhang, Z.; Shi, N.N.; Lu, M.; Stein, A.; Li, C.Y.; Ramanathan, S.; et al. Correlated Perovskites as a New Platform for Super-Broadband-Tunable Photonics. *Adv. Mater.* **2016**, *28*, 9117–9125. [CrossRef]
31. Wan, C.; Zhang, Z.; Salman, J.; King, J.; Xiao, Y.; Yu, Z.; Shahsafi, A.; Wambold, R.; Ramanathan, S.; Kats, M.A. Ultrathin Broad-band Reflective Optical Limiter. *Laser Photonics Rev.* **2021**, *15*, 2100001. [CrossRef]

32. RahimianOmam, Z.; Ghobadi, A.; Khalichi, B.; Ozbay, E. Adaptive thermal camouflage using sub-wavelength phase-change metasurfaces. *J. Phys. D Appl. Phys.* **2023**, *56*, 025104. [CrossRef]
33. Wuttig, M.; Yamada, N. Phase-change materials for rewriteable data storage. *Nat. Mater.* **2007**, *6*, 824–832. [CrossRef] [PubMed]
34. Heßler, A.; Wahl, S.; Leuteritz, T.; Antonopoulos, A.; Stergianou, C.; Schön, C.-F.; Naumann, L.; Eicker, N.; Lewin, M.; Maß, T.W.W.; et al. In3SbTe2 as a programmable nanophotonics material platform for the infrared. *Nat. Commun.* **2021**, *12*, 924. [CrossRef]
35. Zhang, Y.; Chou, J.B.; Li, J.; Li, H.; Du, Q.; Yadav, A.; Zhou, S.; Shalaginov, M.Y.; Fang, Z.; Zhong, H.; et al. Broadband trans-parent optical phase change materials for high-performance nonvolatile photonics. *Nat. Commun.* **2019**, *10*, 4279. [CrossRef]
36. Kim, H.; Osofsky, M.; Prokes, S.M.; Glembocki, O.J.; Piqué, A. Optimization of Al-doped ZnO films for low loss plasmonic materials at telecommunication wavelengths. *Appl. Phys. Lett.* **2013**, *102*, 171103. [CrossRef]
37. Amador-Alvarado, S.; Flores-Camacho, J.M.; Solís-Zamudio, A.; Castro-García, R.; Pérez-Huerta, J.S.; Antúnez-Cerón, E.; Or-tega-Gallegos, J.; Madrigal-Melchor, J.; Agarwal, V.; Ariza-Flores, D. Temperature-dependent infrared ellipsometry of Mo-doped VO2 thin films across the insulator to metal transition. *Sci. Rep.* **2020**, *10*, 8555. [CrossRef] [PubMed]
38. Suleiman, A.O.; Mansouri, S.; Margot, J.; Chaker, M. Tuning VO2 phase stability by a combined effect of Cr doping and oxygen pressure. *Appl. Surf. Sci.* **2022**, *571*, 151267. [CrossRef]
39. Tien, C.-L.; Chiang, C.-Y.; Wang, C.-C.; Lin, S.-C. Optical, Electrical, Structural, and Thermo-Mechanical Properties of Undoped and Tungsten-Doped Vanadium Dioxide Thin Films. *Materials* **2024**, *17*, 2382. [CrossRef] [PubMed]
40. Cheng, Y.; Zhang, X.; Fang, C.; Chen, J.; Su, J.; Wang, Z.; Sun, G.; Liu, D. Synthesis, structure and properties of printable W-doped thermochromic VO2 with a low phase transition temperature. *Ceram. Int.* **2018**, *44*, 20084–20092. [CrossRef]
41. Larciprete, M.C.; Ceneda, D.; Scirè, D.; Mosca, M.; Adorno, D.P.; Dereshgi, S.A.; Macaluso, R.; Voti, R.L.; Sibilia, C.; Cesca, T.; et al. Tunable IR perfect absorbers enabled by tungsten doped VO2 thin films. *APL Mater.* **2023**, *11*, 091107. [CrossRef]
42. Varignon, J.; Grisolia, M.N.; Íñiguez, J.; Barthélémy, A.; Bibes, M. Complete phase diagram of rare-earth nickelates from first-principles. *NPJ Quantum Mater.* **2017**, *2*, 21. [CrossRef]
43. Domínguez, C.; Georgescu, A.B.; Mundet, B.; Zhang, Y.; Fowlie, J.; Mercy, A.; Waelchli, A.; Catalano, S.; Alexander, D.T.L.; Ghosez, P.; et al. Length scales of interfacial coupling between metal and insulator phases in oxides. *Nat. Mater.* **2020**, *19*, 1182–1187. [CrossRef]
44. Yuan, Y.; Kotiuga, M.; Park, T.J.; Patel, R.K.; Ni, Y.; Saha, A.; Zhou, H.; Sadowski, J.T.; Al-Mahboob, A.; Yu, H.; et al. Hydrogen-induced tunable remanent polarization in a perovskite nickelate. *Nat. Commun.* **2024**, *15*, 4717. [CrossRef]
45. Catalano, S.; Gibert, M.; Fowlie, J.; Íñiguez, J.; Triscone, J.-M.; Kreisel, J. Rare-earth nickelates RNiO3: Thin films and hetero-structures. *Rep. Prog. Phys.* **2018**, *81*, 046501. [CrossRef] [PubMed]
46. Chen, J.; Hu, H.; Wang, J.; Yajima, T.; Ge, B.; Ke, X.; Dong, H.; Jiang, Y.; Chen, N. Overcoming synthetic metastabilities and revealing metal-to-insulator transition & thermistor bi-functionalities for d-band correlation perovskite nickelates. *Mater. Hori-zons* **2019**, *6*, 788–795. [CrossRef]
47. Mercy, A.; Bieder, J.; Íñiguez, J.; Ghosez, P. Structurally triggesectionred metal-insulator transition in rare-earth nickelates. *Nat. Com-mun.* **2017**, *8*, 1677. [CrossRef]

Disclaimer/Publisher's Note: The statements, opinions and data contained in all publications are solely those of the individual author(s) and contributor(s) and not of MDPI and/or the editor(s). MDPI and/or the editor(s) disclaim responsibility for any injury to people or property resulting from any ideas, methods, instructions or products referred to in the content.